Analytic calculation for the binding energy of an on-center donor impurity in core/shell/shell quantum dot

M. EL KHOU[*], EL ALAMI IBNOUELGHAZI, D. ABOUELAOUALIM
LN2E, Department of Physics, Faculty of Sciences Semlalia, Cadi Ayaad University, Marrakesh, Morocco

In this study, we present a general analytic solution for any system describing a Core/Shell/Shell Quantum Dot or briefly CSSQD with and without an on-center donor impurity using only one solution wave function build by a linear combination of the Whittaker functions. In the framework of the effective mass approximation, in the conduction band, we apply this general solution wave function on a special case, ZnS/HgS/ZnS multi-shell quantum dot in order to calculate the confinement energy and binding energy for the ground state and several other excited state as well as the probability densities, the results show that the general solution does matches with the reference solutions given by the spherical Bessel function for the impurity-less case, and agrees with the results when the energy is positive when the impurity is present, which are given by the coulomb functions.

1. Introduction

The recent developments in the manufacturing and growth technology allowed us to fabricate low dimensional systems such as the zero dimensional Quantum Dots, which restrict the motion of the charge carriers in all three dimensions. They have been widely utilized for electronic devices due to the fact they can be processed using cost-effective solution-based methods such as spin coating or contact printing [1], as well as their unique electrical and optical properties which can be precisely controlled by adjusting their overall size and thickness [2–6].

Nanocrystals with more than one material, like core/shell quantum dots, enjoy some interesting perks as they offer more parameters to tweak on in order to maximize their electrical and optical properties such as quantum yield [7], they can be synthesized in high-boiling organic solvents, like CdSe/ZnS [8] and CdSe/CdS [9]. Multilayered QD has been studied theoretically by many researchers [10], their electronic properties under some different physical effects have been reported in the literature [11–13].

The study of the impurity states in semiconductor nanostructures was initiated only in early 1980s through the pioneering work of Bastard [14]. The confinement in all three dimensions in QDs causes a reduction of the distance between the electron and the impurity leading an increase in the Coulomb interaction. Bose et al. [15–18] obtained the binding energy of a shallow hydrogenic impurity in spherical QDs. As the interest of impurity doping in nanocrystallites grows, much theoretical works have been carried out on donors in multi-shell QDs employing different methods [19–25], as they study the effect of impurity on the energy spectra in multi-shell nanostructures.

Our main motivation in this work is to find a simple but general wave function solution that is capable of describing simultaneously a Multi-Shell Quantum dot with and without an on-center impurity, no matter what the energy is compared to the barrier potentials of each layer, then apply the general wave function solution on a ZnS/HgS/ZnS core/shell/shell quantum dot to study the binding energy of the confined electron.

2. Theoretical framework

We present in this study an electron confined in an isolated multi-shell quantum dot with inner radii R_1, the first layer thickness Δ_1 and the second layer thickness Δ_2 as shown in Fig. 1.
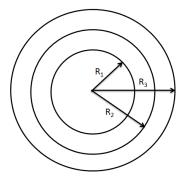

Fig. 1. Cross section of a multi-shell quantum dot

Such a system can be described by solving the time independent Schrodinger equation with a position

dependent effective mass which has the form given by BenDaniel and Duke [26] as follows:

$$-\frac{\hbar^2}{2}\nabla\frac{1}{m_e^*(r)}\nabla\psi + V(r)\psi = E\psi \qquad (1)$$

where the first term is the kinetic energy operator for a position dependent effective mass, $V(r)$ is the confining potential, which binds the electron in a specific region accordingly and E is the total energy Eigen value.

We can write the CSS potential $V(r)$ function with the on-center donor impurity included as a point wise function as follows:

$$V(r)=\begin{cases}V_1 - Ze^2/4\pi\varepsilon_1 r & 0 \le r \le R_1 \\ V_2 - Ze^2/4\pi\varepsilon_2 r & R_1 \le r \le R_2 \\ V_3 - Ze^2/4\pi\varepsilon_3 r & R_2 \le r \le R_3 \\ \infty & r > R_3\end{cases} \qquad (2)$$

And the effective mass is defined in the same manner as:

$$m_i^*(r)=\begin{cases}m_1^* & 0 \le r \le R_1 \\ m_2^* & R_1 \le r \le R_2 \\ m_3^* & R_2 \le r \le R_3\end{cases} \qquad (3)$$

We can solve Eq. (1) by performing a separation of variables, as follows:

$$\Psi_{nlm}(r,\hat{r}) = R_{nl}(r)Y_{lm}(\hat{r}) \qquad (4)$$

This solution allow us to uncouple the three dimensional Schrödinger equation to a simple one dimensional problem, dependent only on the radial component, since the potential used here doesn't break any spherical symmetry, which means the Hamiltonian is invariant under rotation, we proceed by computing the energy Eigen states by solving the radial dependent Schrödinger equation, for each layer, we get three coupled differential equations, which contain a regular singular point at $r = 0$ due to the spherical symmetry, as a result the core wave function will have a singular solution which will be omitted since it have no physical meaning.

$$-\frac{\hbar^2}{2m_i^*}\frac{\partial^2 R(r)}{\partial r^2} - \frac{\hbar^2}{2m_i^*}\frac{2}{r}\frac{\partial R(r)}{\partial r} +$$
$$\frac{\hbar^2}{2m_i^*}\frac{\ell(\ell+1)}{r^2}R(r) + V_i(r)R(r) = ER(r) \qquad (5)$$

Solving Eq. (5) for the core and both shells require three separate wave functions, which need to be linked together by BenDaniel and Duke boundary conditions [26], the functions are given as follows:

$$R(r)=\begin{cases}\psi_c(r) = A_1 f_1^c(k_1 r) & 0 \le r \le R_1 \\ \psi_s(r) = A_2 f_1^s(k_2 r) + B_2 f_2^s(k_2 r) & R_1 \le r \le R_2 \\ \psi_{ss}(r) = A_3 f_1^{ss}(k_3 r) + B_3 f_2^{ss}(k_3 r) & R_2 \le r \le R_3\end{cases} \qquad (6)$$

where A_1, A_2, A_3, B_2, B_3 are normalization constants, the next step is to apply the BenDaniel and Duke boundary conditions on $\psi_c(r)$, $\psi_s(r)$ and $\psi_{ss}(r)$ as follows:

$$\begin{cases}\psi_c(R_1) = \psi_s(R_1) \\ \frac{1}{m_1^*}\frac{d\psi_c(r)}{dr}\bigg|_{r=R_1} = \frac{1}{m_2^*}\frac{d\psi_s(r)}{dr}\bigg|_{r=R_1} \\ \psi_s(R_2) = \psi_{ss}(R_2) \\ \frac{1}{m_2^*}\frac{d\psi_s(r)}{dr}\bigg|_{r=R_2} = \frac{1}{m_3^*}\frac{d\psi_{ss}(r)}{dr}\bigg|_{r=R_2} \\ \psi_{ss}(R_3) = 0\end{cases} \qquad (7)$$

We get after some tedious simplifications a function that host all the properties of the problem and depend on the energy, the energy Eigen values are zeros of this function, it is written as follows:

$$G(E) = \frac{k_1}{m_1^*}F_1^c(k_1 R_1)\alpha_3 - \frac{k_2}{m_2^*}f_1^c(k_1 R_1)\tilde{\alpha}_3 \qquad (8)$$

where we define α_3, $\tilde{\alpha}_3$, $\bar{\alpha}_3$, α_2, $\tilde{\alpha}_2$, α_1 and $\tilde{\alpha}_1$ as follows:

$$\alpha_1 = f_1^{ss}(k_3 R_3)f_2^{ss}(k_3 R_2) - f_1^{ss}(k_3 R_2)f_2^{ss}(k_3 R_3) \qquad (9)$$

$$\tilde{\alpha}_1 = f_1^{ss}(k_3 R_3)F_2^{ss}(k_3 R_2) - F_1^{ss}(k_3 R_2)f_2^{ss}(k_3 R_3) \qquad (10)$$

$$\alpha_2 = \frac{k_2}{m_2^*}F_1^s(k_2 R_2)\alpha_1 - \frac{k_3}{m_3^*}f_1^s(k_2 R_2)\tilde{\alpha}_1 \qquad (11)$$

$$\tilde{\alpha}_2 = \frac{k_2}{m_2^*}F_2^s(k_2 R_2)\alpha_1 - \frac{k_3}{m_3^*}f_2^s(k_2 R_2)\tilde{\alpha}_1 \qquad (12)$$

$$\alpha_3 = f_1^s(k_2 R_1)\tilde{\alpha}_2 - f_2^s(k_2 R_1)\alpha_2 \qquad (13)$$

$$\tilde{\alpha}_3 = F_1^s(k_2 R_1)\tilde{\alpha}_2 - F_2^s(k_2 R_1)\alpha_2 \qquad (14)$$

$$\bar{\alpha}_3 = f_1^s(k_2 R_2)\tilde{\alpha}_2 - f_2^s(k_2 R_2)\alpha_2 \qquad (15)$$

All the capital letters functions are first order derivative as shown below:

$$F_i^j(r) = \frac{df_i^j(x)}{dx}\bigg|_{x=r} \qquad (16)$$

To compute the analytical electron's energy levels we need to solve this transcendental equation where the energy E is the unknown:

$$\text{Re}\big(G(E)\big) = 0 \qquad (17)$$

The wave function normalization constants are as follows:

$$
\begin{cases}
A_2 = f_1^c(k_1 R_1)\dfrac{\widetilde{\alpha}_2}{\alpha_3}A_1 \\[2mm]
B_2 = -f_1^c(k_1 R_1)\dfrac{\alpha_2}{\alpha_3}A_1 \\[2mm]
A_3 = -f_1^c(k_1 R_1)f_2^{ss}(k_3 R_3)\dfrac{\overline{\alpha}_3}{\alpha_1\alpha_3}A_1 \\[2mm]
B_3 = f_1^c(k_1 R_1)f_1^{ss}(k_3 R_3)\dfrac{\overline{\alpha}_3}{\alpha_1\alpha_3}A_1
\end{cases}
\qquad (18)
$$

One normalization constant A_1 still remains unidentified, which can be found by applying the normalization condition as follows:

$$\int_0^{R_1}|\psi_c|^2 r^2 dr + \int_{R_1}^{R_2}|\psi_s|^2 r^2 dr + \int_{R_2}^{R_3}|\psi_{ss}|^2 r^2 dr = 1 \quad (19)$$

We can see that the transcendental equation (17) depend only on the set of functions $f_j^i(r)$ which in return depend directly on the potential $V(r)$, when successfully solved, we'll be able to obtain all the energy levels of the electron confined in the quantum dot, this procedure gives us a big advantage if we'd like to add more shells to our quantum dot, as we only need to find its corresponding linkage function $G(E)$ and add more functions which we already have.

Consider we have a spherical multi-shell quantum dot with and without an impurity at its center; the quintuplet solution functions for all energies are given by:

$$
\begin{cases}
f_1^c(r) = \dfrac{1}{r}M_{\frac{Z}{a_1 k_1},\ell+\frac{1}{2}}(2r) \\[3mm]
f_1^s(r) = \dfrac{1}{r}M_{\frac{Z}{a_2 k_2},\ell+\frac{1}{2}}(2r) \\[3mm]
f_2^s(r) = \dfrac{1}{r}W_{\frac{Z}{a_2 k_2},\ell+\frac{1}{2}}(2r) \\[3mm]
f_1^{ss}(r) = \dfrac{1}{r}M_{\frac{Z}{a_3 k_3},\ell+\frac{1}{2}}(2r) \\[3mm]
f_2^{ss}(r) = \dfrac{1}{r}W_{\frac{Z}{a_3 k_3},\ell+\frac{1}{2}}(2r)
\end{cases}
\qquad (20)
$$

where $M_{n,\ell}(r)$ and $W_{n,\ell}(r)$ are the two linearly independent Whittaker functions, while a_i and k_i are respectively the Bohr radius and wave vector respectively for the core and the shells, defined as:

$$a_i = \frac{4\pi\varepsilon_i\hbar^2}{m_i^* e^2} \qquad k_i = \sqrt{\frac{2m_i^*(V_i - E)}{\hbar^2}}$$

The general solution (20) is capable of covering both cases where the donor impurity at the center is in effect ($Z=1$) and the other case where it's absent ($Z=0$), moreover for any value of the energy E compared to V_i without the need to use any other complicated functions such as the Confluent Hypergeometric function or the Coulomb function [27–29]. However there is an important condition to fulfill when the impurity is absent, we have to make Z so close but not entirely equal to zero, in this simulation we take $Z=5\times10^{-18}$ as it give us accurate results compared to the reference solutions where we usually use the spherical Bessel functions, we get an energy difference in the vicinity of $\Delta E\approx10^{-16}$eV. It is also important to take cautious from other unwanted zeros of the transcendental equation (17) that sometimes emerges so close to the wanted result in some extreme scenarios when the value of the electron's energy is in the neighborhood of the barrier potentials ($E \approx V_1, V_2$ and V_3) or in some extreme condition when a layer width is chosen extremely small compare to the others, which can make finding the proper eigenvalue a little bit challenging, however this issue can be solved sometimes by looking at the probability density.

The Binding energy can be calculated as the expectation value of the donor impurity potential using the solution wave function in Eq. (4), or simply by using this formula:

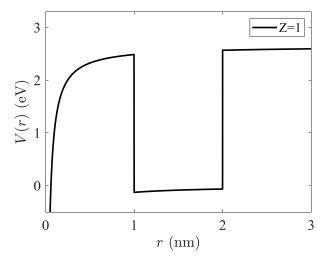$$E_{nlm}^{(b)} = E_{nlm}(Z=0) - E_{nlm}(Z=1) \qquad (21)$$

Fig. 2. ZnS/HgS/ZnS CSS Quantum dot potential with the impurity at the center

Now let's apply the general solution (20) to a special case, ZnS/HgS/ZnS CSSQD, with a specific potential as shown in Fig. 2. And compute the electron's confinement

energy as well as its binding energy for different core radii R_1 and shells thicknesses.

3. Results and discussion

In this section, we will apply the general solution to a ZnS/HgS/ZnS multi-shell quantum dot, in order to compute the variation of the confinement energy for the ground state (1s) and other excited states with the influence of a donor impurity at the center, then we deduce their corresponding binding energy using Eq. (21), trying various cases of the core radii R_1, first thickness Δ_1 and second thickness Δ_2 in order to test the consistency of the solution for geometric adjustment, and finally we plot the probability densities. For this purpose we take the confinement potential in the first shell as Energy reference, making it equal $V_2 = 0eV$ since the bottom of the conduction band is located in HgS in comparison with ZnS which is much higher, while the core and the second shell are $V_1 = V_3 = 2.65eV$ [30,31], for the effective mass of the electron in the conduction band we have $m_2^* = 0.04m_0$ [30] for HgS and $m_1^* = m_3^* = 0.28m_0$ [32] for ZnS, where m_0 is the free electron mass, as for the dielectric constant we have $\varepsilon_2 = 11.4\varepsilon_0$ [30] for HgS, while $\varepsilon_1 = 8.9\varepsilon_0$ [32] for ZnS, where ε_0 is the vacuum permittivity.

We begin our discussion by looking at Fig. 3 as it illustrate the variation of the confinement ground state energy (1s) and multiple other excited states with respect to HgS thickness Δ_1, in a fixed size quantum dot $R_3 = 5$ nm, all sharing the same principal quantum number ($n=1$) in Fig. 3a and ($n=2$) in Fig. 3b, while making the core radii and the outer thickness vary equally $R_1 = \Delta_2$, as we vary the HgS layer thickness Δ_1 from zero to 5 nm, we observe a noticeable decrease in the confinement energy especially for the (1s) state, this effect is simply a result of the decrease of the magnitude of the probability density at the center of the QD, as the thickness of HgS rises, more suitable states emerges with less spatial restrictions, as the opposite to the surrounding material ZnS which is growing slimmer with less states for the electron to occupy, this is also true when we make ($n=2$) as shown in Fig. 3b, we see a different energy variation behavior for the three lowest states (2s), (2p) and (2d) as we increase thickness Δ_1, from 0 to approximately 1.9 nm the confinement energy experience a slight change, then decrease noticeably until around 4.6 nm as we observe once again a rising in the confinement energy, for the (2f) state we see that the confinement energy increase until HgS thickness reaches $\Delta_1 = 3.1$ nm, since part of the probability density still remain in the ZnS core and outer shell where the confinement is getting high, then the energy get low as this remaining of the probability density in ZnS material completely travel to HgS which is getting quite wide in comparison.

Fig. 3. Variation of electron's confinement energy as a function of HgS thickness Δ_1 for $R_3 = 5$ nm (color online)
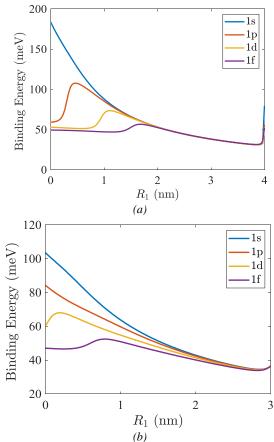

Fig. 4. Variation the binding energy as a function of the core radii R_1 for a fixed HgS thickness of (a) $\Delta_1 = 1$ nm and (b) $\Delta_1 = 2$ nm in a $R_3 = 5$ nm (color online)

In Fig. 4 we have the variation of the binding energy for several electronic states with ($n=1$) for a fixed HgS thickness Δ_1 and outer radius $R_3=5$nm, while we vary the core radii R_1 from 0 to $R_3-\Delta_1$. Fig. 4a shows the case where we choose $\Delta_1= 1$ nm, as the core radii R_1 increases, the binding energy decreases since the probability density moves away from the center as it mostly located within HgS layer, until we reach approximately $\Delta_2= 0.1$ nm where the binding energy suddenly increases, which can be explained by the fact that the probability density spread back to the center once again. We see a different pattern when ℓ is non null, as we observe an increase followed by a decrease while reaching a maximum value which is well visible for the (2p) and (2d) when we're in high confinement $\Delta_1= 1$ nm. When we loosen up the thickness of HgS to $\Delta_1= 2$ nm, we see a similar variation as before however with a lower energy and less defined bumps.
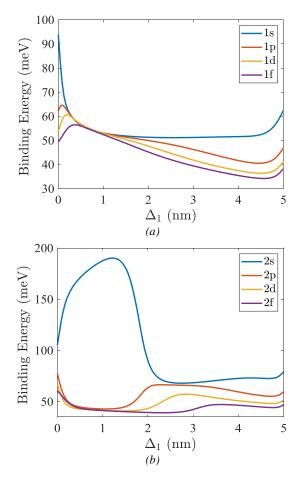
stabilization at approximately 51 meV starting from $\Delta_1=1$ nm until 4.5 nm where the probability density decrease and spread with a steady rate, finally we see that the binding energy rises toward the end as the probability density increases once again at the center to match the case of a ZnS quantum dot with no HgS included. For the (2s) state, we observe a noticeable increase of the binding energy summiting at 190.2 meV around $\Delta_1= 1.22$ nm, followed by a decrease to a minimum of 68 meV at 2.75 nm the increases with a steady rate until we have a complete HgS quantum dot, for states with ℓ different than zero, we see a similar behavior for all three states (1p), (1d) and (1f) as the binding energy increases to a maximum value then decreases until HgS thickness reaches 4.6 nm where it rises up again as the probability density matches up with a quantum dot with only one material. We see the same thing occur for (2p), (2d) and (2f) states, as they seem to share the same pattern for the binding energy, we focus here on the (2p) state as we observe an even sharper decrease when we increase Δ_1 gradually until it reaches the global minimum at $\Delta_1=1$nm at 42.8 meV then we see an increases in the binding energy to a local maximum of 66.4 meV at $\Delta_1=2.2$nm, and then we see a steady slow rate decrease in the binding energy until a local minimum with the value of 55.2 meV at $\Delta_1=4.7$nm and increase for the remaining of the curve.

(a)

(b)

Fig. 5. Variation of the binding energy for the ground state and several excited state (a) as a function of HgS thickness Δ_1 while fixing $R_3=5$ nm (color online)

Fig. 5 shows us the effect of varying the HgS thickness Δ_1 on the binding energy for multiple states in a fixed total radius $R_3= 5$ nm, at $\Delta_1=0$nm we have a quantum dot with only ZnS molecules, as we increase Δ_1 gradually which introduce HgS particles from the $R_3/2$, we observe a sharp decrease in the (1s) state binding energy which is accompanied with a fast probability density decrease at the center of the quantum dot, followed by an energy
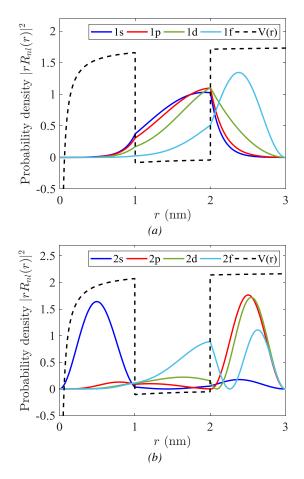

(a)

(b)

Fig. 6. Probability density in a ZnS/HgS/ZnS CSS Quantum Dot under the influence of an on-center impurity (Z=1) (color onine)

In Fig. 6 we present the electron's probability density for multiple confinement states in a ZnS/HgS/ZnS quantum dot with a hydrogenic donor impurity at the center, for a fixed thickness layout (R_1= 1.0nm, Δ_1= 1.0nm, Δ_2=1.0nm), we observe that for the lowest state energy, the (1s) and (1p) states probability density are situated inside HgS, since their energy is less than the band offset potential 2.65eV, which host the states with the lowest energy possible, while (1d) state is slightly higher with 2.74eV, which is enough energy to make a transition from HgS to the outer ZnS.

4. Conclusion

In this study, we give a general analytic solution to the Schrödinger equations describing a spherical Core/Shell/Shell Quantum dot with and without the influence of an on-center donor impurity, using only one general wave function solution realized using the Whittaker functions. We apply the solution obtained to compute the electronic properties of an electron confined in the ZnS/HgS/ZnS multi-shell quantum dot, we have shown the effect of varying the inner radiis of the multi-shell quantum dot layers on the electronic properties. We observed that the results stayed consistent throughout the simulation for any care radii R_1 or inner and outer shell thickness, for both cases when the donor impurity is absent (Z=0) and present (Z=1), the solution was also tested for other effective mass and offset potential configurations, and both results matches.

References

[1] L. A. Kim, P. O. Anikeeva, S. A. Coe-Sullivan, J. S. Steckel, M. G. Bawendi, V. Bulovic, Contact printing of quantum dot light-emitting devices, Nano Lett. **8**(12), 4513 (2008).

[2] D. Bera, L. Qian, T. K. Tseng, P. H. Holloway, Materials **3** , 2260 (2010).

[3] W. Y. Ji, P. T. Jing, W. Xu, X. Yuan, Y. J. Wang, J. L. Zhao, A. K.-Y. Jen, Appl. Phys. Lett. **103**, 053106 (2013).

[4] J.-S. Lee, J. Cho, C. Lee, I. Kim, J. Park, Y.-M. Kim, H. Shin, J. Lee, F. Caruso, Nat. Nanotech. **2**, 790 (2007).

[5] Y. Ko, H. Baek, Y. Kim, M. Yoon, J. Cho, ACS Nano **7**, 143 (2013).

[6] D. H. Kim, W. K. Kim, S. J. Woo, C. Wu, T. W. Kim, Org. Electron. **51**, 156 (2017).

[7] H. Borchert, D. Dorfs, C. McGinley, S. Adam, T. Moller, H. Weller, A. Eychmüller, J. Phys. Chem. B **107**, 7486 (2003).

[8] D. Dorfs, H. Henschel, J. Kolny, A. Eychmüller, J. Phys. Chem. B **108**, 1578 (2004).

[9] P. Reiss, S. Carayon, J. Bleuse, A. Pron, Synthetic Metals **139**, 649 (2003).

[10] C.-Y. Hsieh, D.-S. Chuu, J. Physics: Condensed Matter **12**, 8641 (2000).

[11] S. Aktas, F. K. Boz, Physica E **40**, 753 (2008).

[12] F. K. Boz, S. Aktas, A. Bilekkaya, S. E. Okan, Appl. Surf. Sci. **255**, 6561 (2009).

[13] F. K. Boz, S. Aktas, A. Bilekkaya, S. E. Okan, Appl. Surf. Sci. **256**, 3832 (2010).

[14] G. Bastard, Phys. Rev. B **24**, 4714 (1981).

[15] C. Bose, Physica E **4**, 180 (1999).

[16] C. Bose, C. K. Sarkar, Solid State Electron. **42**, 1661 (1998).

[17] C. Bose, C. K. Sarkar, Physica B **253**, 238 (1998).

[18] C. Bose, J. Appl. Phys. **83**, 3089 (1998).

[19] M. Cristea, E. C. Niculescu, Eur. Phys. J. B **85**, 191 (2012).

[20] V. A. Holovatsky, O. M. Makhanets, O. M. Voitsekhivska, Physica E **41**, 1522 (2009).

[21] V. A. Holovatsky, I. B. Bernik, O. M. Voitsekhivska, Acta Phys. Pol. A **125**, 93 (2014).

[22] V. A. Holovatsky, I. B. Frankiv, J. Optoelectron. Adv. M. **15**(1-2), 88 (2013).

[23] V. I. Boichuk, R. Ya. Leshko, I. V. Bilynskyi, L. M. Turyanska, Condens. Matter Phys. **15**, 33702 (2012).

[24] V. I. Boichuk, I. V. Bilynskyi, R. Ya. Leshko, L. M. Turyanska, Physica E **44**, 476 (2011).

[25] V. I. Boichuk, I. V. Bilynskyi, R. Ya. Leshko, Condens. Matter Phys. **13**, 13702 (2010).

[26] D. J. BenDaniel, C. B. Duke, Phys. Rev. **152**, 683 (1966).

[27] M.-C. Lin, D.-S. Chuu, J. Appl. Phys. **90**, 2886 (2001).

[28] D. Stojanovic, R. Kostic, Acta. Phys. Pol. A **120**(2), 234 (2011).

[29] D. Schooss, A. Mews, A. Eychmüller, H. Weller, Phys. Rev. B **49**(24), 17072 (1994).

[30] M. Royo, J. Planelles, M. Pi, Phy. Rev. B **75**, 033302 (2007).

[31] W. Bao, Sachuronggui, F.-Y. Qiu, Chin. Phy. B **25**(12), 127102 (2016).

[32] B. A. Ebrahimipour, H. R. Askari, A. B. Ramezani, Superlattice Microstruct. **97**, 495 (2016).

_____
*Corresponding author: elkhoumorad@gmail.com